Assessing the connectivity of a regional fractured aquifer based on a hydraulic conductivity field reversed by multi-well pumping tests and numerical groundwater flow modeling

Journal:	*Journal of Earth Science*
Manuscript ID	JES-12-2021-0672.R2
Manuscript Type:	Original Article
Date Submitted by the Author:	19-Apr-2022
Complete List of Authors:	Lin, Jingjing; China University of Geosciences; Yangtze River Basin Ecological Environment Monitoring and Scientific Research Center, Yangtze River Basin Ecological Environment Supervision and Administration Bureau, Ministry of Ecological Environment Ma, Rui; China University of Geosciences Sun, Ziyong; China University of Geosciences Tang, Liansong; China University of Geosciences
Keywords:	Numerical modeling, aquifer connectivity, preferential flow channel,

	minimum hydraulic resistance, multi-well pumping test
Speciality:	Hydrogeochemistry < Geochemistry

Assessing the connectivity of a regional fractured aquifer based on a hydraulic conductivity field reversed by multi-well pumping tests and numerical groundwater flow modeling

JingJing Lin[1,2], Rui Ma [1*], Ziyong Sun[1], Liansong Tang[1]

[1]School of Environmental Studies & State Key Laboratory of Biogeology and Environmental Geology, China University of Geosciences, 430074 Wuhan, China

[2]Yangtze River Basin Ecological Environment Monitoring and Scientific Research Center,Yangtze River Basin Ecological Environment Supervision and Administration Bureau, Ministry of Ecological Environment, 430014 Wuhan, China

*Corresponding author: Rui Ma, rma@cug.edu.cn

Submitted to *Journal of Earth Science*

December 2021

Abstract:

Aquifer connectivity could greatly affect groundwater flow and further control the contaminant transport in fractured medium. However, assessing connectivity of fractured aquifer at regional scales is still a challenge because such connectivity is difficult to measure directly. This study proposed a framework for assessing connectivity of a fractured aquifer, with Qitaihe area, Heilongjiang Province, northeastern China as an illustrating study area. The 3-D finite difference numerical models were established to interpret the results of three multi-well pumping tests and inversely estimate the distribution of hydraulic conductivity (K) in the fractured aquifer. A static connectivity metric of the minimum hydraulic resistance (MHR) was calculated, based on the optimized K-field, to evaluate the hydraulic connectivity in the aquifer, and the corresponding least resistance paths (LRPs) were identified. The results indicate that a better horizontal connectivity in the fractured aquifer in the northeastern and middle parts than in the southwestern part of the study area. The identified LRP indicated that the preferential flow channels at regional scales were controlled mainly by aquifer connectivity instead of local high-K zones.The results of this study can provide a method for aquifer connectivity estimation at regional scales.

Keywords:

Numerical modeling; aquifer connectivity; preferential flow channel; minimum hydraulic resistance; multi-well pumping test

1. Introduction

The connections among high hydraulic conductivity (K) zones usually form channels or preferential flow paths providing the main flow flux and solute particles in fractured aquifers (Tyukhova et al., 2015; Le Goc et al., 2010) that could result in contaminants having heterogeneous flow fluxes and differing transport times (Bianchi et al., 2018; Bianchi et al., 2017; Pool and Dentz, 2017; Russo, 2016; Pedretti et al., 2013). Although fractured aquifers have matrixes with a high volume of impervious rock that produces a relatively small effective porosity, average groundwater flow velocities can be significant when fractures are well connected (Persaud et al., 2018). In this context, assessing the connectivity of and accurately characterizing preferential flow channels may be particularly important for groundwater management and contamination remediation in fractured media.

Most studies on the connectivity of fractured aquifers have focused on local scales using slug tests (e.g., Guiltinan and Becker, 2015; Guihéneuf et al., 2014; Gellasch et al., 2013, 2014). Assessing the connectivity of fractured aquifers at regional scales remains a challenge because it is difficult to measure directly (Ishii, 2018). Given that connectivity is an intrinsic feature of aquifer heterogeneity (Tyukhova and Willmann, 2016), which is a function of contrasts between high- and low-*K* zones, information on connectivity in fractured media can be related to the spatial distribution of hydraulic conductivity at a regional scale. Pumping tests can be conducted to characterize the *K*-field at the field scale (e.g., Fischer et al., 2018; Freixas et al., 2017), while numerical modeling has proven to be effective for interpreting these and inversely estimating the spatial distribution of hydraulic conductivity in fractured aquifers. For example, Qian et al. (2009) successfully inverted the hydraulic parameters of a fractured rock matrix by developing a 3-D transient flow model with two sequential pumping tests at the Zhangji well field in northern China. Qian et al. (2014) developed a 2-D finite element transient flow model for a fractured medium in Zinder, Niger, and successfully obtained hydraulic parameters based on a multi-well pumping test.

Several measures have been proposed to quantitatively evaluate the hydraulic connectivity of aquifers (e.g., Le Goc et al., 2010; Knudby and Carrera, 2005). Renard and Allard (2013) classified these measures into static metrics, as a function of the *K*-field, and dynamic metrics representing hydrodynamic processes such as flow and solute transport. One of the main advantages of static metrics is that the properties and connectivity structure of an aquifer can be related directly without considering dynamic flow and transport processes. Tyukhova et al. (2015) defined the hydraulic connectivity in an aquifer system as path(s) with the lowest hydraulic resistance (HR) between two boundaries; they also proposed a numerical method to delineate the connectivity structures of heterogeneous media formed by path(s) with the least resistance based on hydraulic conductivity information alone. Later, Tyukhova and Willmann (2016) derived static connectivity metrics from HR using information from the *K*-field and validated their capability to predict effective flow and solute transport for a wide range of 2-D *K*-fields with various connectivity structures. This idea was expanded upon by Rizzo and Barros (2017), who proposed using the minimum hydraulic resistance (MHR) to identify the least resistance path (LRP) and presented an efficient algorithm based on graph theory with which to derive the MHR and identify the LRP. Their results also indicated that the early arrival time of solute and the fastest transport path were strongly correlated with the MHR and LRP. Rizzo and Barros (2019) then used this algorithm to further explore the uncertainty of the MHR as affected by the geological structures of the subsurface medium and domain dimension in a stochastic framework, and proposed an iterative data sampling strategy to reduce uncertainties with identifying LRPs. The MHR and LRP methods show great promise as ways to explore how to estimate the connectivity of aquifers in hydrogeological studies. However, the connectivity metric of the MHR and the method of identifying LRPs have, in their current formulations, been applied mainly to synthetic *K*-fields. Although aquifer connectivity is particularly important for exploiting groundwater resources and assessing the risk from contaminants at real field sites, few investigations have been conducted– until now–to characterize aquifer connectivity based on LRPs, particularly at a regional scale. This may have been due to the difficulty of obtaining an accurate model of the structure of the *K*-field on a large field scale.

To fill this knowledge gap, the objective of this study was to derive the hydraulic connectivity of a regional fractured aquifer with using *K*-field obtained from multi-well pumping tests and numerical modeling. Three multi-well pumping tests were conducted at the site of a fractured aquifer in the Qitaihe area, Heilongjiang Province, northeastern China, and 3-D saturated transient groundwater flow models were created and then calibrated using data from the multi-well pumping tests. The *K*-field in the fractured aquifer was obtained based on the calibrated model and used to compute the MHRs and identify the corresponding LRPs at three groundwater extraction zones. Finally, the horizontal connectivity of the fractured aquifers was evaluated based on the computed MHRs and identified LRPs. This research is expected to provide a framework for evaluating the static connectivity metrics of MHRs and identifying the preferential flow channel in a real, regional fractured aquifer. Furthermore, the results will contribute to water resource management and the assessment of risks environmental contamination in the study area.

2. Study area

2.1 General setting

The study area is in the Qitaihe area, an important industrial and agricultural district of Heilongjiang Province in northeastern China, and covers an area of approximately 390.6 km^2 (Fig. 1a). It runs northeast to southwest and is a valley plain with elevations ranging from 160-220 m above sea level (m.a.s.l.). Its overall topography is high in the northeast and low in the southwest. There is a hilly area with an elevation of 500-690 m.a.s.l outside the southeastern and northwestern boundaries of the valley plain. The Woken River and Taoshan Reservoir are the main surface water bodies in the study area. The Woken River, which is part of the Songhua River system, flows through the valley plain from the northeast to the southwest. The Taoshan Reservoir, with an area of 26.3 km^2, occupies the southwestern part of the study area and was formed by damming the Woken River. For a long time, the Taoshan Reservoir was the main water source for the industrial, domestic, and agricultural demands in the Qitaihe area.

2.2 Geological setting

Figure 1a presents a map of the location, with a corresponding hydrogeological cross section shown in Fig. 1b. Quaternary unconsolidated sediment (Q), consisting mainly of fine sand and sandy gravel, are distributed along the valley plain at a thickness of 5-10 m. The formation underlying the Q is a Cretaceous (K) system that can be divided into two systems-the Early and Middle Cretaceous (K_{1-2h}) Houshigou Group and the Early Cretaceous (K_{1c}) Chengzihe Group-from top to bottom. The Houshigou Group (K_{1-2h}) is composed of siltstone and medium-coarse sandstone and conglomerate, with a thickness of ~180 m. The Chengzihe Group (K_{1c}) consists of medium-fine sandstone and siltstone with a thickness of ~120 m.

Owing to the compressional diagenesis in the Yanshan tectonic movement, fractures were well developed in the K_{1-2h} sandstone layer and poorly developed in the K_{1c} sandstone layer in the valley plain. According to Qi (2015), the fractures in the K_{1-2h} sandstone layer developed in many directions, such as SN, EW, NNE, NNE, or NE and so on, of which the EW-trending, NE-trending, and NW-trending fractures are the main regional structures. Qi (2015) inferred, based on the results of geophysical and hydrogeological surveys, that the fractures in the K_{1-2h} sandstone layer formed a series of fractured zones along the extension direction of the valley plain. Mudstone with a low permeability underlies the K_{1c} sandstone in the valley plain. In the hilly area, the K system bedrock consists of sandstone with extremely poorly developed fractures with several outcrops. A series of faults with good transmissibility developed vertically along the southeastern and northwestern boundaries of the study area (Fig. 1b).

2.3 Hydrogeological setting

Three aquifers were recognized in the valley plain: (1) the Q porous groundwater system distributed along the lenghth of the valley, with a well-specific yield of 0-1000 m^3/d; (2) the sandstone fissure groundwater system in the K_{1-2h} formation with a relatively high well-specific yield of 1000-3000 m^3/d; and (3) the sandstone fissure groundwater system in the K_{1c} formation with a well-specific yield of 100-1000 m^3/d. In the K bedrock system outside the valley plain, the well-specific yield was 0-100 m^3/d.

Regionally, groundwater flows from northeast to southwest and from lateral boundaries into the valley plain with a mean hydraulic gradient of $\sim 7 \times 10^{-4}$ (Fig. 2). With the local topography as a control, the depth of the groundwater is ~15 m below the surface (m.b.s) in the northern and central parts of the valley plain and ~5 m.b.s in the southern part of the valley plain (near the Taoshan Reservoir). Under natural conditions, the groundwater level in the study area would have been higher than the water level of the Taoshan Reservoir year-round (Qi, 2015).

The main groundwater system recharge sources in the valley plain are precipitation infiltration, leakage from the Woken River, and lateral influxes from hilly areas at the southeastern, northwestern, and northeastern boundaries. Groundwater discharge includes loss to evaporation, surface water, and lateral outflow through the topographically deep southwestern boundary. The lateral outflow from the southwestern boundary only occurs below a depth of 110 m because the impermeable dam (see Fig. 1a) was built from the surface to a depth of 110 m. Using a traditional hydrogeological survey and water balance calculation, Qi (2015) estimated the following contributions of different recharge resources to the groundwater system in the valley plain: precipitation infiltration, $\sim 270.24 \times 10^4$ m^3/a; lateral inflow, $\sim 1027.43 \times 10^4$ m^3/a; and leakage from the river, $\sim 508.23 \times 10^4$ m^3/a. This study also calculated the groundwater discharge to the Taoshan Reservoir (~1001.5 × 10^4 m^3/a), loss from evaporation (~1206.2 × 10^4 m^3/a), and the lateral outflow through the southwestern boundary (~28.93 m^3/a).

3. Multi-well pumping tests

In 2012, the Qitaihe area suffered from an extreme drought that sharply decreased the stored capacity of the Taoshan Reservoir. Therefore, to alleviate water shortages, the groundwater in the fractured aquifer located upstream of the Taoshan Reservoir was selected as a new source of water to supply the Qitaihe area. As Fig. 2 shows, three groundwater extraction zones were established in the study area and 58 fully screened wells with screen depths of 168-188 m were drilled in the K_{1-2h} formation by the 904 Hydrogeological and Geologic Engineering Institute (904 HGEI) of Heilongjiang Province, China (Table 1, Fig. 2). The wellhead elevation, well depth, and thickness of the aquifers penetrated by these boreholes is given in Table 1. Subsequently, three multi-well pumping tests-referred to as tests 1, 2, and 3-were conducted by the 904 HGEI in these groundwater extraction zones (at well groups 1, 2, and 3); these were used to assess the quantity of water available as an emergency supply and obtain the hydraulic parameters of the aquifer. The motivations of the long-time extraction and monitoring (Fig. 3) were to ensure the groundwater level reaching a stable state and provide sufficient database for the model calibration.

Test 1 was conducted from 15:00 4/20/2013 to 06:00 AM 5/12/2013, and involved 17 fully screened wells at all. Among them, groundwater from 15 wells were pumped simultaneously, while the monitors of groundwater level were conducted in all 17 wells (Fig. 2). The response of groundwater level to the extraction is shown in the Fig. 3a. The total volume of groundwater extracted from the 15 pumping wells per day was 23,092.8 m^3/d, with each of these wells maintaining a constant pumping rate ranging from 614.16-1,937.52 m^3/d

(Table 1). All pumping wells were operated for 17.79 days and the groundwater levels was monitored continuously for 22.21 days (Fig. 3a).

Test 2 was carried out from 06:00 AM on May 10 to 06:00 AM on May 30, 2013. As shown in Fig. 2, during the pumping test, 23 fully screened wells were used, which contains 20 pumping wells, while the groundwater level was observed at all 23 wells from the beginning (Fig. 3b). The total pumping rate of groundwater extracted from the 20 pumping wells was 32,148.72 m^3/d, with each well keeping a steady pumping rate between 1,456.8 m^3/d and 1,744.08 m^3/d (Table 1). The groundwater was exploited for 17 days, and the monitor of groundwater levels last for 22.83 days (Fig. 3b).

Test 3 started from 06:00 AM on June 1, 2013, invoking 18 fully screened wells. Groundwater was pumped simultaneously from 15 wells (Fig. 2). Groundwater levels of all the 18 wells were monitored continuously (Fig. 3c). The total extraction rate of the 15 pumping wells reached 24,338.88 m^3/d, of which the maximum pumping rate was 2,025.36 m^3/d, and the minimum pumping rate was 628.08 m^3/d (Table 1). The pumping continued for 17 days, and groundwater levels were observed for 22.83 days (Fig. 3c).

4. Numerical model development and analysis methods

4.1 Development of a numerical model

In order to consider the potential impact of the heterogeneity induced by zonal hydrogeological units and dual layer structure (two adjacent aquifers with different degree of fracture development) on the groundwater flow system, a 3D numerical model with two layers was constructed to simulate the three pumping tests and inversely estimate the hydraulic conductivity of the fractured aquifer in the study area.

4.1.1 Hydrogeological concept model

Based on the geological and hydrogeological settings presented in Section 2, the lateral boundaries of the study area-except for the southwestern part-were treated as inflow boundaries in the model because of the good transmissibility of the faults. The upper 110 m of the southwestern boundary was treated as a no-flow boundary because the upper aquifer had no direct hydraulic connection with the Taoshan Reservoir due to the presence of the dam; the lower part of the southwestern boundary was regarded as an outflow boundary. The bottom of the model was characterized as a no-flow boundary. The main discharge during the pumping tests was groundwater abstraction. Precipitation, evaporation, Taoshan Reservoir, and Woken River were defined as the top boundaries of the model.

The actual aquifer was generalized using a two-layer hydrogeological conceptual model to ensure that the different parts of the fractured aquifer were accounted for. The two layers were ~180 m and ~120 m thick, respectively, and the first model layer was treated as an aquifer with good permeability, while the second model layer was treated as an aquifer with low permeability. In the model, the Q aquifer and the upper K ($K_{1\text{-}2h}$) sandstone layers with well-developed fractures were treated as the first model layer for the following reasons. (1) The Q aquifer, at 5-10 m thick, was much thinner than the K fractured aquifer (~160 m thick) (Table 1); however, the water in the aquifers were generally less than 5 m deep. Furthermore, as described above, the specific yield from the Q aquifer was much lower than that of the fracture aquifer. Thus, the thin Q aquifer contributed little to water storage. (2) The observation wells were all fully screened, vertically penetrating the entire fracture aquifer such that no monitoring data were available to separately calibrate the hydraulic parameters in the porous Q aquifer. Thus, it would not have been meaningful to treat the Q aquifer as a separate layer in the model.

4.1.2 Mathematical model

There are two main approaches for describing the groundwater flow in fractured media: the equivalent porous media method and the discrete fracture network method. Miotliński et al. (2011) noted that the latter is particularly recommended for small-scale studies in which the properties and spatial orientation of fractures are known. Their literature review also concluded that if matrix diffusion processes are unimportant, equivalent porous media can represent the solute transport in both sedimentary and crystalline rock aquifers. This study focused on groundwater flow at a regional scale and no data were available for the fracture network in the study area. Therefore, the equivalent porous medium approach was applied to the numerical model to generalize the fractured aquifer. A similar modeling process has already been applied successfully to characterize solute transport processes (Jarrahi et al., 2019; Abusaada and Sauter, 2013; Berkowitz and Braester, 1988) and groundwater flow through other fractured aquifers (Zhang et al., 2017; Khoei et al., 2016; Qian et al., 2014; White, 2011; Qian et al., 2009; Lemieux et al. 2009; White, 2006).

Based on the above generalization, the groundwater flow in the study area obeys Darcy's law. And then, three-dimensional finite-element models have been used for simulating groundwater flow in the fractured media. For the completeness of presentation, the groundwater flow governing equation is given as:

$$\frac{\partial}{\partial x}\left(K_x\frac{\partial h}{\partial x}\right)+\frac{\partial}{\partial y}\left(K_y\frac{\partial h}{\partial y}\right)+\frac{\partial}{\partial z}\left(K_z\frac{\partial h}{\partial z}\right)+w=S_s\frac{\partial h}{\partial t}(x,y,z)\in\Omega \quad (4.1.1)$$

Where h is the hydraulic head (L); x, y, z are the coordinates in the x, y, and z directions, respectively (L); K_x, K_y and K_z are the hydraulic conductivities in direction x, y, and z, respectively (L/T); w is the discharged or recharged flux per unit aquifer wolume (T^{-1}); t is time (T); S_s is specific storage (L^{-1}); Ω is the domain of study.

4.1.3 Numerical modeling

The finite difference models were built using the software MODFLOW 2005 (Harbaugh, 2005) code to simulate the 3-D, transient, and saturated groundwater flow during the three pumping tests. The model covered a spacing range of 23600 m in the X direction, 24200 m in the Y direction, and ~300 m in the Z direction. The horizontal spacing of the model grid varied from 50–400 m and was refined at the locations of the well groups. Vertically, the model grids were divided into two layers ~180 m and ~120 m thick, respectively. Undulations in the elevation of the ground surface were characterized by borehole data from 58 wells (Table 1) and digital elevation model data for the study area. The elevation of the bottom of the first model layer was interpolated, with drilling data, using the Kriging method (Table 1). The bottom of the second model layer was assumed to be horizontal. The three multi-well pumping tests were all simulated for 22.21 days. The three transient simulations were divided into hourly stress periods.

The initial distribution of the groundwater level (shown in Fig. 2) was interpolated, according to data observed from the 58 wells immediately before the multi-well pumping tests started, using the Kriging method. The influx from the northeastern boundary was estimated using the Darcy equation based on the average groundwater hydraulic gradient in the study area (Fig. 2) and hydraulic conductivity near the boundary. The outflow from the southwestern boundary and the influx from the other lateral boundaries were set up according to results from previous studies (Qi, 2015). Considering that the lateral influx boundaries were related to rainfall events, the model considered seasonal variations in the influxes based on the intra-annual distribution of precipitation in the study area.

The Woken River was defined using the RIVER package in MODFLOW 2005 and the river stage was defined using data from Qi (2015). The riverbed conductance was initially calculated based on the thickness, vertical hydraulic conductivity, and width of the riverbed;

it was subsequently calibrated. There was no outflow from the Taoshan Reservoir through the dam, and the reservoir was recharged by groundwater year-round (Qi, 2015). The reservoir was also simulated using the RIVER package because there were only slight fluctuations in the reservoir stage throughout the simulation period. The stage of the reservoir monitored during the simulation period was input into the model.

Precipitation recharge was defined using RECHARGE packages. The infiltration rates of precipitation during the simulation periods (April, May, and June) were initially estimated using monthly precipitation and the infiltration coefficient provided by the 904 HGEI (Qi, 2015). A similar method was used to calculate the average evaporation rate for each month in the EVAPORATION packages. The seasonal precipitation infiltration and evaporation were subsequently calibrated using a groundwater flow model based on one-year data during a period during which the pumping tests did not take place.

A set of initial hydraulic conductivity and specific yield values calculated using the Theis equation and Cooper-Jacob graphical method based on data from 19 single-well pumping tests, were provided by the 904 HGEI. The parameters were interpolated over the entire region in the first model layer using the Kriging method. For the area of well groups 1, 2, and 3, the initial value of K_x ranged from 0.5-1.3 m/d, 1.1-1.3 m/d, and 1.3-1.8 m/d, respectively, with mean S_y values of 0.2, 0.5, and 0.2, respectively; for the area of the Taoshan Reservoir, the initial K_x and S_y values were 1.3 m/d and 0.2, respectively. The K_z/K_x values were both initially set to uniform values of 0.1. The same anisotropy ratio was used by Miotliński et al. (2011) to simulate the flow and solute transport processes in a siltstone-sandstone fractured aquifer; they also used the equivalent porous medium method. Givening the fractures are mainly developed along the valley plain, in other words, the permeability of X direction is better than that of Y direction, thus the K_y/K_x values were both set to 0.5. The initial hydraulic conductivity values of the second layer were set to be one-tenth of that of the first layer due to its low permeability. These ratios and hydraulic parameters used for the different model layers were subsequently calibrated during the model calibration process.

4.2 Methods of computing MHR and identifying LRP

According to the concept of MHR proposed by Rizzo and Barros (2017), for a given aquifer domain R^n (with n=2 or 3 denoting the spatial dimensionality), given a source point $S \in R^n$ and a given arrival point $T \in R^n$, the set of all the possible paths connecting S to T can be defined as $\mathcal{P}_S^T$. To computing the MHR and delineating the LRP between the given point S and T, the HRs of the given aquifer domain R^n need to be calculated firstly based on the K-field distribution (Rizzo and Barros, 2019; Rizzo and Barros, 2017; Tyukhova and Willmann, 2016).

Following the concept proposed by Rizzo and Barros (2019, 2017), for each path $\Gamma \in \mathcal{P}_S^T$, the corresponding HR, $\mathcal{R}_\Gamma$, can be defined as a line integral as follows:

$$\mathcal{R}_\Gamma = \int_\Gamma \frac{1}{K} d\gamma \qquad (4.2.1)$$

where $\mathcal{R}_\Gamma$ is the HR along the path Γ; γ is the unit vector along the path Γ; K is the hydraulic conductivity in unit vector γ.

Based on these calculated HRs, we adopted the method proposed by Rizzo and Barros (2019, 2017) to define the MHR from a point S to T as follows:

$$\mathcal{R}_s(T) = \min_{\Gamma \in \mathcal{P}_S^T} \mathcal{R}_\Gamma \qquad (4.2.2)$$

where $\mathcal{R}_s(T)$ is the MHR within $\mathcal{P}_S^T$ between the point S and T. Correspondingly, the path $\hat{\Gamma} \in \mathcal{P}_S^T$ that meets $\mathcal{R}_{\hat{\Gamma}} = \mathcal{R}_s(T)$ is defined as the LRP connecting the given point S and T.

Generally, calculating the MHR or finding the LRP in a continuum framework has great challenges due to it requires to explore all the possible paths connecting two points.

Therefore, a graph theory-based procedure developed by Rizzo and Barros (2017) using Dijkstra's algorithm (Dijkstra, 1959) was introduced in this study to allow the computation of the MHR and find the LRP that connects two boundaries in a specified *K*-field. In brief, the value $\mathcal{R}_s(T)$ defined in equation 4.2.2 is the solution of a minimization problem in a graph framework. Appropriately, the Djkstra's algorithm (Dijkstra, 1959) which was initially developed to calculate the shortest path between two given points in graph theory can solve the above problem, and it was successfully applied in the study of Rizzo and Barros (2019, 2017).

A detailed description of the methodelogy for computing the MHR or finding the LRP in a given aquifer domain can be found in Rizzo and Barros (2017). Here only the major steps are outlined. For a given *K*-field, it must be discretized such that each cell *i* is characterized by a hydraulic conductivity value K_i. This domain partition is the same used in finite difference methods. The coordinates of the center of each cell represents a vertex. Two cells are considered neighbors if they share a common face or a common corner. Two cells sharing a common face or a common corner are treated as neighbors. Each vertex is connected to a neighbor vertex through an edge. The weight w_e associated to an edge e connecting two neighboring vertices v_i and v_j can be defined as:

$$w_e = \frac{|r_{ij}|}{K_i} + \frac{|r_{ji}|}{K_j} \qquad (4.2.3)$$

Where $|r_{ij}|$ is the length of the segment connecting the vertexs of cells *i* and *j*. All vertices and edges in the given domain form a set *V* and a set *E*, respectively, and then they are defined as a *hydraulic resistance graph* *G*(*V*, *E*). Using the HR graph, we can find an approximation of HR and MHR described in eauation 4.2.1 and 4.2.2. Combing eauation 4.1.3, for each path Γ in a discrete hydraulic conductivity field, the corresponding HR and MHR becomes:

$$\mathcal{R}_\Gamma = \int_\Gamma \frac{1}{K} d\gamma = \sum_{e\in\Gamma} w_e \tag{4.2.4}$$

$$\mathcal{R}_s(T) = \min_{\Gamma\in\mathcal{P}_S^T} \sum_{e\in\Gamma} w_e \tag{4.2.5}$$

For all possible paths connecting two given points, the one that has the minimum sum of w_e can be found effectively using Dijkstra's algorithm. Therefore, the LRP connecting two given points can be extracted with the MHR. Similarly, the LRP connecting two boundaries can also be found effectively by setting a series of source and arrival points.

5. Results and discussion

5.1 Model calibration

To obtain reasonable values for the seasonal lateral influx, precipitation infiltration, and evaporation, a regional groundwater flow model with the setup described above was built and run for one year during which there were no pumping tests; this was done before calibrating the models used to analyze the pumping tests. This model was calibrated with hydrographs at the seven long-term monitoring wells, and the seasonal lateral influx, precipitation, and evaporation were estimated based on the calibrated model. As these results are not closely related to the objective of this study, they are not given in this paper.

To optimize the initial parameters, the models used to simulate the pumping tests were calibrated to match simulated values with observations. Therefore, because the screens of the pumping and observation wells used in the three pumping tests were in the first model layer, the calibration was implemented mainly in this layer. The effect of the hydraulic parameters in the second model layer on the change in groundwater level in the first layer was also tested, and the parameters adjusted correspondingly. According to our test, the groundwater level was much more sensitive to K_x and K_z in the first layer than in the second layer during pumping tests 2 and 3, maybe due to the low permeability and fractures poorly developed in the second model layer. In addition, according to the results of sensitivity analysis, the groundwater level was no sensitive to K_y in both two model layers, which is probably due to the narrow width of the Woken River, resulting in less groundwater recharge in the Y direction during the multi-well pumping test. Therefore, the model calibration focused on the K_x and K_z of the first model layer.

The hydraulic parameters were first adjusted manually, by trial and error, to fit the observed and simulated groundwater levels; following this, the automated parameter estimation code was used to optimize the values of these parameters. During the calibration processes, the effects K_x and K_z on drawdown evolutions existed throughout the pumping period. For Test 1, K_x and K_z jointly control the rate of groundwater level decline at the early stage, while the terminal groundwater level was mainly controlled by K_x . On the contrary, for Test 2 and Test 3, the decline and recovery rates of groundwater level in early and later period were mainly controlled by K_z, whereas K_x determined the stable groundwater level in the middle period.

Figure 3 shows that the match between the simulated and observed groundwater levels was generally good for most monitoring wells during the three pumping tests. Most of the observations for each test fell on or close to the 1:1 line on the graph of the observed vs. simulated hydraulic level (Fig. 4). Some disparities present between the observed and simulated data might have been caused by the high heterogeneity of the fractured aquifer system; that could not be characterized in detail. For the 5,184 observations in test 1, the absolute residual mean (ARM) between the observed and simulated heads was 0.197 m and the root mean square (RMSE) was 0.343 m. For test 2, which included 12,282 observations, the ARM was 0.378 m and the RMSE was 0.537 m. For test 3, in which there were 9,612 observations, the ARM and RMSE were 0.247 m and 0.392 m, respectively. Generally, the

391 ARM and RMSE for the three tests were less than 0.5 m and quite low relative to the maximum groundwater level variations of ~10 m, ~22 m, and ~30 m for tests 1, 2, and 3, respectively. This indicates that the simulated and observed heads were well matched and the calibrated model can be considered reliable.

395 ***5.2 Spatial structure of K-field***

396 After the model was calibrated, the distribution of the optimized K_x and K_z of the first model layer with well-developed fractures was mapped (Fig. 5). The study area was divided into 49 specific zones based on numbers of boreholes and differences in water yield properties and geomorphic type, and the K_x and K_z values of each zone are given in Table 2. The values of K_x and K_z range from 0.01-3 m/d and 0.1-5 m/d, respectively. The values of K_x are higher than those of K_z in the areas of well groups 2 and 3 (Fig. 5 and Table 2), suggesting a better hydraulic connection in the horizontal direction than in the vertical direction. Overall, the values of K inversed in this study are consistent, in terms of their orders of magnitude, with the results from the single-well pumping tests conducted by the 904-HGEI.

406 Generally, the values of K_x in most zones are between 0.1 m/d and 1 m/d (Fig. 5a). However, there are a few zones local to the area of well group 2 with higher K_x values and a few zones in the areas of well groups 1 and 3 with lower K_x values. The slightly decreasing trend of K_x from the plain to the Taoshan Reservoir suggests a decrease in the horizontal permeability of the fractured aquifer from northeast to southwest of the study area. This is consistent with the variation in the characteristics of the K values provided by the 904-HGEI (see Section 2). These K_z values were used to merge the 49 zones into two types, those with K_z values ranging from 0.1-1 m/d and 1-10 m/d (Fig. 5b). Almost the entirety of well group 1 area and half that of well group 3 have K_z values of 1-10 m/d, while most of well group 2

area has a K_z value of 0.1-1 m/d. For the fracture aquifers, the complex fracture networks can lead to highly heterogeneous K field at both vertical and horizontal direction. As shown in Figure 5, the value of K_z can higher than that of K_x in the area of well group 1 and well gorup 3, which is the distinct characteristic of fracture aquifer and different with that of porous aquifer. Overall, the fractured aquifer had higher K_z values in the upper reaches of the valley plain (0.1-1 m/d) are significantly smaller than that in the lower reaches (1-10 m/d). Thus, it can be inferred that the vertical permeability of the fractured aquifer increased from northeast to southwest in the study area. In other words, the downstream region of the $K_{1\text{-}2h}$ sandstone layer (the first model layer) has better vertical connectivity, and the vertical connectivity of the fractured aquifer gradually increase from upstream to downstream.

5.3 Connectivity of the fractured aquifer

The calibrated K values from the numerical models, shown above, were used to construct the HR field of the fractured aquifer in the three well group areas. According to the results of sensitivity analysis, the groundwater level was less sensitive to K values of the second layer, maybe due to its low permeability. Therefore, the flow dynamic in the study area is mainly controlled by the hydraulic conductivity in the $K_{1\text{-}2h}$ sandstone layer. To evaluate the hydraulic connectivity in the aquifer, a static connectivity metric of the minimum hydraulic resistance (MHR) was calculated based on the K_x fields in the first layer ($K_{1\text{-}2h}$ sandstone).

The connectivity of three 2-D K_x fields corresponding to the three well group areas were selected for evaluation using the method presented in section 4.2. The locations of the three rectangular areas selected are shown in Fig. 5; they are referred to as sections 1, 2, and 3 and have sizes of 5000 m × 1800 m, 4400 m × 1800 m, and 4400 m × 2400 m, respectively. The three sections were divided into 200 m × 200 m grids as shown in Fig. 6. The values of K_x obtained from the model calibration were smoothed in the range of the three sections, after which the smoothed K_x values were assigned to each grid. Grids outside the numerical model domain given were assigned a uniform K_x value of 1×10^{-6} m/d, which is low enough for groundwater to bypass them. Finally, the HRs were calculated with the corresponding K_x fields for each section using Eq. (1). The HR field for each section was used to extract the MHR via Eq. (2) and the LRP connecting two opposite boundaries was obtained using Dijkstra's algorithm.

The MHRs calculated for the fractured aquifer between the two opposite boundaries of each section are shown in Fig. 6. Among these, the MHR for section 1 is the greatest (94.83), indicating that the fractured aquifer in groundwater extraction region 1 is relatively poorly connected. In comparison, the fractured aquifers in groundwater extraction regions 2 and 3, with MHRs of 29.48 and 28.7, respectively, are more connected. This shows that the connectivity of the fractured aquifer gradually decreases from northeast to southwest in the study area. This finding is consistent with the qualitative description of fracture development by Qi (2015), whose hydrogeological and geophysical investigations indicated that there may have been NNE-trending fracture zones at a small scale in groundwater extraction regions 2 and 3 that enhanced the horizontal connectivity of the aquifers in these regions.

Figure 6 also illustrates the LRP identified as connecting the northeastern boundary to the southwestern boundary of each of the three sections. Generally, the locations of the three LRPs are all close to the western boundaries of the aquifer domain and the LRPs from the three sections connect to each other, although they were identified separately and formed a preferential channel through the regional aquifer in the study area. Although some local grids had relatively high K_x values, the LRPs do not pass through them. This suggests that the groundwater flow at the regional scale may have been controlled mainly by aquifer connectivity rather than local hydraulic conductivity. Studies at the Wilcox aquifer, Texas (Fogg, 1986) and Livingston site, Louisiana (Hanor, 1993), USA reached similar conclusions.

Interestingly, the LRPs are similar to the trajectory of the Woken River. This may be attributed to the evolution of regional tectonics. According to Qi (2015), since the Neogene, under the influence of the Pacific plate movement, the crust sank as a whole; and then fracture zones on both sides were formed under the action of the NW-SE tensile stress. After the negative topography was formed by formation depression, the Woken River developed along the fault structure. During this process, under the influence of the revival of old structures, the NE-trending fractures were cut and merged by NNE-trending fractures, the connection of which induced the spatial distribution of the LRPs.

The delineation of LRPs linked to preferential flow channels can provide valuable support for locating groundwater source regions and predicting contaminant migration. To improve the efficiency of extracting groundwater from the fractured aquifer that serves as a new source of water for the Qitaihe area, we recommend selecting boreholes along the LRPs as pumping wells. Additionally, the leading front of a solute plume has been found to be strongly correlated with its preferential flow path (Rizzo and Barros, 2017; Tyukhova and Willmann, 2016; Knudby and Carrera, 2006). Thus, the structure of the LRPs delineated in this study can also be used to estimate the early arrival time of a particular contaminant and can be applied to assess the risk of environmental contamination.

5.4 Limitations and future studies

Calculating the MHR and delineating the LRP are greatly dependent on accurate estimations of the *K*-field. In the two-layer numerical model in our study, K_z controls the groundwater flow rate from the second model layer to the first and then into the wells during the pumping tests. Given the uncertainty of K_z in the second model layer owing to a lack of observation data, the calibrated K_z in the first model layer may also be subject to uncertainty. Nevertheless, this study focused on determining the horizontal connectivity of the fractured aquifer based on the spatial distribution of K_x in the first model layer; this result should remain unchanged even given any uncertainty in K_z. Additionally, the results of evaluating the LRP from this study showed that it is consistent the findings from hydrogeological and geophysical investigations by Qi (2015). This, in turn, provided good evidence that the spatial distribution of K_x estimated using the method in this study is reasonable. However, the vertical connectivity in the fractured aquifer and the effects thereof on the estimation of the K-field are worth investigating in future studies.

6. Summary and conclusion

The connectivity of fractured aquifers, even those in rock matrixes with low permeability and spread over a wide area, could greatly affect groundwater flow paths and contaminant transport. Although the methods for calculating static metrics and characterizing hydraulic connectivity based on the information from the K-field have been both proposed and advanced in recent years, they are still investigated only rarely at real field sites, particularly at regional scales, owing to the difficulties in obtaining the structure of the K-field. This study provides a framework for estimating aquifer connectivity based on the spatial distribution of hydraulic conductivity (K) in a regional fractured aquifer. Taking the Qitaihe area in Heilongjiang Province, China as the study area, we established numerical groundwater flow models with which to analyze multi-well pumping tests, the results of which we used to inversely estimate the K-field of the fractured aquifer. Finally, the MHRs for the 2-D aquifer between the northeastern boundary and southwestern section near the Taoshan Reservoir in the study area were calculated based on the inverse K_x-field, and the corresponding LRPs were identified.

The optimized horizontal hydraulic conductivity (K_x) of the fractured aquifer range 0.01-3 m/d, decreasing generally from the northeast to the southwest in the study area. The MHR of the aquifer increased from the northeast to the southwest part of the study area, suggesting better connectivity in the northern part compared to the southwestern part. These results can be seen in the distribution trends of the fractures that developed in the study area. A connected preferential channel crossing the aquifer in the study area was indicated by LRPs derived from MHRs calculations, which implies that this connected channel may mainly control the regional groundwater flow, although local high hydraulic conductivity zones also exist. This should be carefully considered when designing groundwater exploitation plans and predicting the early arrival times of a specified contaminant for risk assessment. Therefore, because the connectivity assessment method with the high computational efficiency used in this study can be flexibly applied at field sites without dimensional and scale restrictions, it can provide a reference for other hydrogeological studies focusing on field scale aquifer connectivity.

ACKNOWLEDGEMENTS

This work was financially funded by the National Natural Science Foundation of China (grants no. 41722208 and 41521001), Natural Sciences Foundation of Hubei Province of China (2019CFA013), and the 111 Program (State Administration of Foreign Experts Affairs & the Ministry of Education of China, grant B18049). We thank the 904 Hydrogeological and Geological Engineering Institute of Heilongjiang Province in China for providing the multi-well pumping test data and other relevant hydrogeological data.

REFERENCES CITED

Abusaada, M., Sauter, M., 2013. Studying the flow dynamics of a karst aquifer system with an equivalent porous medium model. *Groundwater*, 51(4), 641-650.

Berkowitz, B., Bear, J., Braester, C., 1988. Continuum models for contaminant transport in fractured porous formations. *Water Resources Research*, 24(8), 1225-1236.

Bianchi, M., Pedretti, D., 2017. Geological entropy and solute transport in heterogeneous porous media. *Water Resources Research*, 53(6), 4691-4708.

Bianchi, M., Pedretti, D., 2018. An Entrogram-Based Approach to Describe Spatial Heterogeneity with Applications to Solute Transport in Porous Media. *Water Resources Research*, 54(7), 4432-4448.

Dijkstra, E. W., 1959. A note on two problems in connexion with graphs. *Numerische Mathematik*, 1(1), 269-271.

Fischer, P., Jardani, A., Jourde, H., et al., 2018. Harmonic pumping tomography applied to image the hydraulic properties and interpret the connectivity of a karstic and fractured aquifer (Lez aquifer, France). *Advances in Water Resources*, 119, 227-244.

Fogg, G. E., 1986. Groundwater flow and sand body interconnectedness in a thick, multiple aquifer system. *Water Resources Research*, 22, 679-694.

Freixas, G., Fernàndez-Garcia, D., Sanchez-Vila, X., 2017. Stochastic estimation of hydraulic transmissivity fields using flow connectivity indicator data. *Water Resources Research*, 53(1), 602-618.

Gellasch, C. A., Bradbury, K. R., Hart, D. J., et al., 2013. Characterization of fracture connectivity in a siliciclastic bedrock aquifer near a public supply well (Wisconsin, USA). *Hydrogeology Journal*, 21(2), 383-399.

Gellasch, C. A., Wang, H. F., Bradbury, K. R., et al., 2014. Reverse water-level fluctuations associated with fracture connectivity. *Groundwater*, 52(1), 105-117.

Guihéneuf, N., Boisson, A., Bour, O., et al., 2014. Groundwater flows in weathered crystalline rocks: Impact of piezometric variations and depth-dependent fracture connectivity. *Journal of Hydrology*, 511, 320-334.

Guiltinan, E., Becker, M. W., 2015. Measuring well hydraulic connectivity in fractured bedrock using periodic slug tests. *Journal of Hydrology*, 521, 100-107.

Harbaugh, A.W., 2005. MODFLOW-2005, the U.S. Geological Survey modular ground-water model the Ground-Water Flow Process: U.S. Geological Survey Techniques and Methods 6-A16.

Hanor, J.S., 1993. Effective hydraulic conductivity of fractured clay beds at a hazardous waste landfill, Louisiana Gulf Coast. *Water Resources Research*, 29(11), 3691-3698.

Ishii, E., 2018. Assessment of hydraulic connectivity of fractures in mudstones by single-borehole investigations. *Water Resources Research*, 54(5), 3335-3356.

Jarrahi, M., Moore, K. R., Holländer, H. M., 2019. Comparison of solute/heat transport in fractured formations using discrete fracture and equivalent porous media modeling at the reservoir scale. *Physics and Chemistry of the Earth*, Parts A/B/C, 113, 14-21.

Knudby, C., Carrera, J., 2005. On the relationship between indicators of geostatistical, flow and transport connectivity. *Advances in Water Resources*, 28(4), 405-421.

Khoei, A. R., Hosseini, N., Mohammadnejad, T., 2016. Numerical modeling of two-phase fluid flow in deformable fractured porous media using the extended finite element method and an equivalent continuum model. *Advances in Water Resources*, 94, 510-528.

Miotliński, K., Dillon, P. J., Pavelic, P., Cook, P. G., Page, D. W., Levett, K., 2011. Recovery of injected freshwater to differentiate fracture flow in a low-permeability brackish aquifer. *Journal of Hydrology*, 409(1-2), 273-282.

Lemieux, J. M., Kirkwood, D., Therrien, R., 2009. Fracture network analysis of the St-Eustache quarry, Quebec, Canada, for groundwater resources management. *Canadian Geotechnical Journal*, 46(7), 828-841.

Le Goc, R., de Dreuzy, J. R., Davy, P., 2010. Statistical characteristics of flow as indicators of channeling in heterogeneous porous and fractured media. *Advances in Water Resources*, 33(3), 257-269.

Pool, M., Dentz, M.., 2017. Effects of heterogeneity, connectivity and density variations on mixing and chemical reactions under temporally fluctuating flow conditions and the formation of reaction patterns. *Water Resources Research*, 54(1), 186-204.

Persaud, E., Levison, J., Pehme, P., et al., 2018. Cross-hole fracture connectivity assessed using hydraulic responses during liner installations in crystalline bedrock boreholes. *Journal of Hydrology*, 556, 233-246.

Pedretti, D., Fernmndez-Garcia, D., Bolster, D., Sanchez-Vila, X., 2013. On the formation of breakthrough curves tailing during convergent flow tracer tests in three-dimensional heterogeneous aquifers. *Water Resources Research*, 49, 4157-4173. https://doi.org/10.1002/wrcr. 20330.

Qi, F., 2015. Hydrogeology of Groundwater Storage in Near-Reservoir Bedrock Fissure Zones: [Dissertation]. China University of Geosciences, Wuhan. (in Chinese)

Qian, J., Zhan, H., Wu, J., et al., 2009. What can be learned from sequential multi-well pumping tests in fracture-karst media? A case study in Zhangji, China. *Hydrogeology Journal*, 17(7), 1749-1760.

Qian, J., Zhou, X., Zhan, H., et al., 2014. Numerical simulation and evaluation of groundwater resources in a fractured chalk aquifer: a case study in Zinder well field, Niger. *Environmental Earth Sciences*, 72(8), 3053-3065.

Renard, P., Allard, D., 2013. Connectivity metrics for subsurface flow and transport. *Advances in Water Resources*, 51, 168-196.

Rizzo, C. B., De Barros, F. P. J., 2017. Minimum hydraulic resistance and least resistance path in heterogeneous porous media. *Water Resources Research*, 53(10), 8596-8613.

Rizzo, C. B., Barros, F. P. J. D., 2019. Minimum hydraulic resistance uncertainty and the development of a connectivity-based iterative sampling strategy. *Water Resources Research*, 55(7), 5593-5611.

Russo, D., 2016. On the effect of connectivity on solute transport in spatially heterogeneous combined unsaturated-saturated flow systems. *Water Resources Research*, 51(5), 3525-3542.

Tyukhova, A. R., Kinzelbach, W., Willmann, M., 2015. Delineation of connectivity structures in 2-D heterogeneous hydraulic conductivity fields. *Water Resources Research*, 51(7), 5846-5854.

Tyukhova, A. R., Willmann, M., 2016. Connectivity metrics based on the path of smallest resistance. *Advances in Water Resources*, 88, 14-20.

White, W. B., 2006. Fifty years of karst hydrology and hydrogeology: 1953-2003. *Special Paper of the Geological Society of America*, 404(1), 139-152.

White, W. B., 2011. A brief history of karst hydrogeology: contributions of the NSS. *Journal of Cave & Karst Studies*, 69(1), 13-26.

Zhang, K., Zhang, X., Zhang, L., et al., 2017. Inversion of fractures based on equivalent continuous medium model of fractured reservoirs. *Journal of Petroleum Science & Engineering*, 151, 496-506.

Tables

Table 1 Statistics on the wells and pumping rates for three multi-well pumping tests (NA means data is not available)

Test No.	Full-screen well ID	Wellhead elevation (m.a.s.l.)	Well Depth (m)	Thickness of Q aquifer (m)	Thickness of K_{1-2h} aquifer (m)	Pumping rate (m^3/d)
Test 1	zk8	177.37	185	9.4	175.6	1398.24
	zk9	177.694	183	10.1	172.9	1428.96
	zk10	178.130	183	8.7	174.3	1646.16
	zk11	177.134	185	8.8	176.2	1551.84
	zk12	177.974	185	9.4	175.6	1640.16
	zk18	176.477	180	9.5	170.5	1571.76
	zk20	180.270	180	8.8	171.2	1551.12
	zk21	180.916	180.3	6.9	173.4	614.16
	zk22	180.239	180.5	10.1	170.4	1937.52
	zk27	180.644	180	9.5	170.5	1679.76
	zk28	180.914	180	6.9	173.1	1546.08
	zk29	180.536	180	10	170	1606.56
	zk35	181.428	180	7	173	1673.76
	zk36	181.659	180	6.9	173.1	1676.64
	sj01	176.357	NA	NA	NA	1570.08
	sj02	NA	NA	NA	NA	0
	zk2	NA	180	10.2	169.8	0
Test 2	zk84	187.219	181	8.7	172.8	1702.56
	zk85	186.468	181	10.1	170.9	1477.2
	zk86	186.753	181.10	6.9	174.2	1744.08
	zk87	186.378	180.1	6.9	173.2	1609.2
	zk91	187.481	180	9.8	170.2	1558.08
	zk92	187.576	180.2	6.9	173.3	1584.24
	zk93	187.826	181	6.9	174.1	1730.4
	zk94	188.167	180	6.9	173.1	1539.84
	zk95	187.565	180	9.4	170.6	1525.2
	zk98	188.075	181	10.1	170.9	1734.48
	zk99	188.307	180	6.9	173.1	1614.96
	zk100	187.879	180	6.9	173.1	1456.8
	zk101	187.235	180.2	10.1	170.1	1665.12
	zk103	188.064	175	8.8	166.2	1643.52
	zk104	188.279	182	9.5	172.5	1476.72
	zk105	188.718	171	9.1	161.9	1610.16
	zk106	188.755	166	9.9	156.1	1739.04
	zk107	188.707	180.1	9.5	170.6	1583.52
	zk108	187.690	180.1	8.7	171.4	1576.8
	zk111	187.707	180	7	173	1576.8
	zk81	186.710	180	10.1	169.9	0
	zk115	187.936	180	10.6	169.4	0
	G02	NA	NA	NA	NA	0
Test 3	zk47	183.117	163	10.1	152.9	1446.48

	zk48	183.566	180.4	10.1	170.3	1704.24
	zk53	183.937	173	8.7	164.3	1756.32
	zk54	183.848	175	8.8	166.2	1783.2
	zk55	185.203	180	6.9	173.1	1745.76
	zk56	184.987	180	6.9	173.1	2025.36
	zk58	184.114	126.15	6.9	119.25	1762.56
	zk62	182.988	180	7	173	1535.04
	zk63	184.927	180	8.7	171.3	1788
	zk64	184.632	180	8.8	171.2	1782.24
	zk65	185.423	183	8.7	174.3	628.08
	zk66	185.998	181	6.9	174.1	1685.52
	zk67	185.510	180	9.5	170.5	1442.16
	zk68	185.118	180	9.8	170.2	1617.84
	zk69	185.205	180	9.7	170.3	1636.08
	Zk41	182.835	180	6.9	173.1	0
	zk61	183.001	180	6.9	173.1	0
	Zk76	186.912	180	6.9	173.1	0

Table 2 The values of the optimized hydraulic conductivity (*K*) in 49 zones as shown in Fig. 5.

Zone No.	K_x (m/d)	K_y (m/d)	K_z (m/d)	Zone No.	K_x (m/d)	K_y (m/d)	K_z (m/d)
1	1	0.50	1	26	0.28	0.14	0.5
2	0.7	0.35	1	27	0.027	0.01	0.1
3	0.5	0.25	0.3	28	1.3	0.65	0.5
4	0.4	0.20	0.2	29	0.25	0.13	0.1
5	3	1.50	0.9	30	0.7	0.35	5
6	1.8	0.90	0.2	31	0.6	0.30	5
7	0.25	0.13	0.25	32	0.15	0.08	5
8	2	1.00	0.2	33	0.001	0.00	4
9	0.2	0.10	0.2	34	0.3	0.15	5
10	0.6	0.30	0.2	35	1	0.50	5
11	0.7	0.35	0.2	36	0.21	0.11	0.5
12	0.5	0.25	0.6	37	0.41	0.21	1
13	1	0.50	1	38	0.01	0.01	4.5
14	0.15	0.08	0.2	39	0.01	0.01	5
15	0.3	0.15	0.2	40	0.15	0.08	5
16	0.65	0.33	0.2	41	0.1	0.05	3.5
17	0.2	0.10	0.5	42	0.2	0.10	5
18	3	1.50	0.2	43	0.5	0.25	5
19	1	0.50	0.5	44	0.01	0.01	5
20	0.5	0.25	0.3	45	0.02	0.01	0.9
21	0.6	0.30	0.3	46	0.14	0.07	1
22	0.2	0.10	2	47	0.35	0.18	3.5
23	0.75	0.38	0.5	48	0.1	0.05	3.2
24	1	0.50	0.5	49	0.1	0.05	0.1
25	0.25	0.13	0.5				

Figures Captions

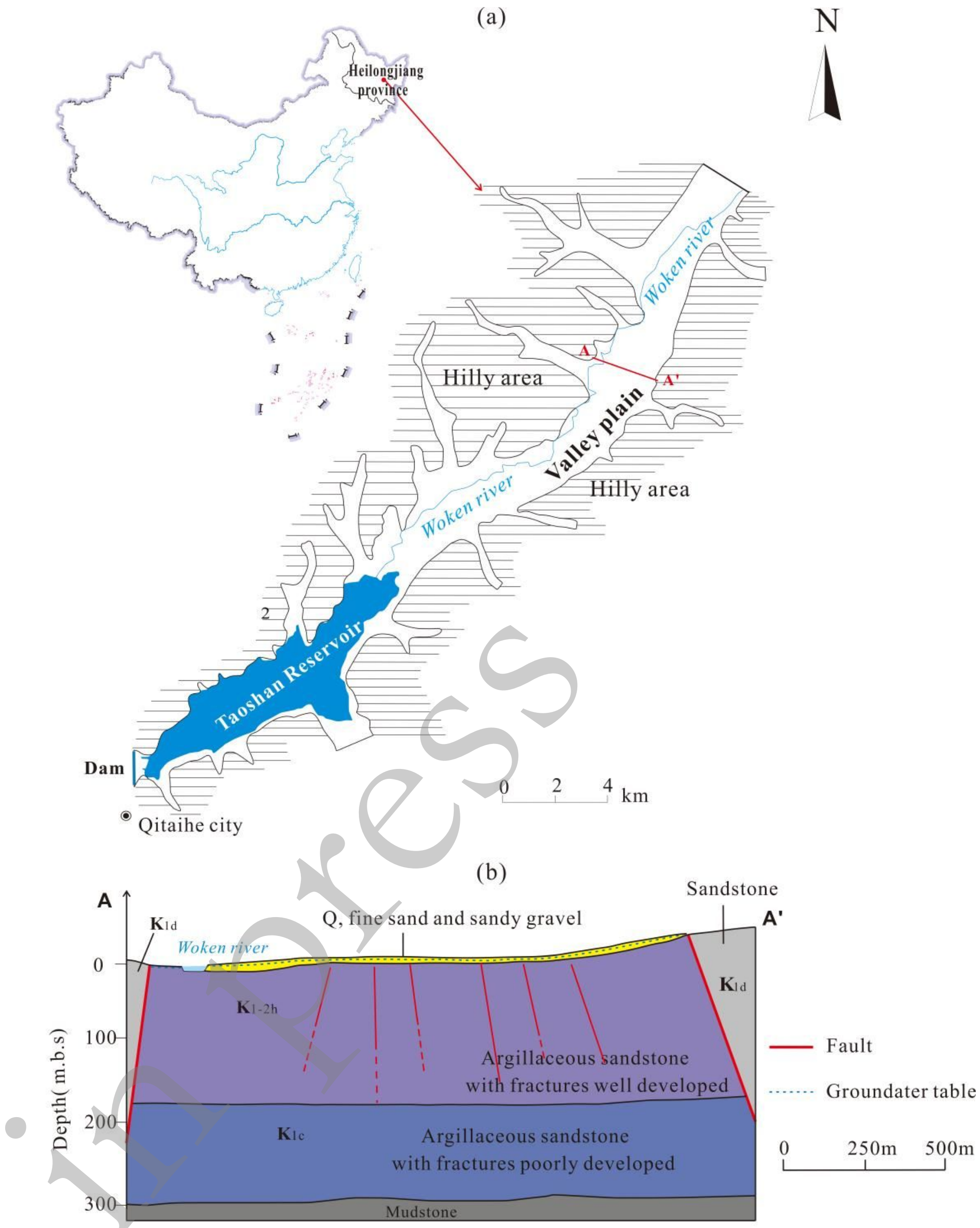

Figure 1. (a) The location of the study area in Heilongjiang Province, China; and (b) the hydrogeological profile of section A-A' (modified from Qi (2015)). Q: Quaternary; K: Cretaceous; $K_{1\text{-}2h}$: Early and Middle Cretaceous Houshigou Group; K_{1c}: Early Cretaceous Chengzihe Group; K_{1d}: Early Cretaceous Didao Group; m.b.s: meters below surface.

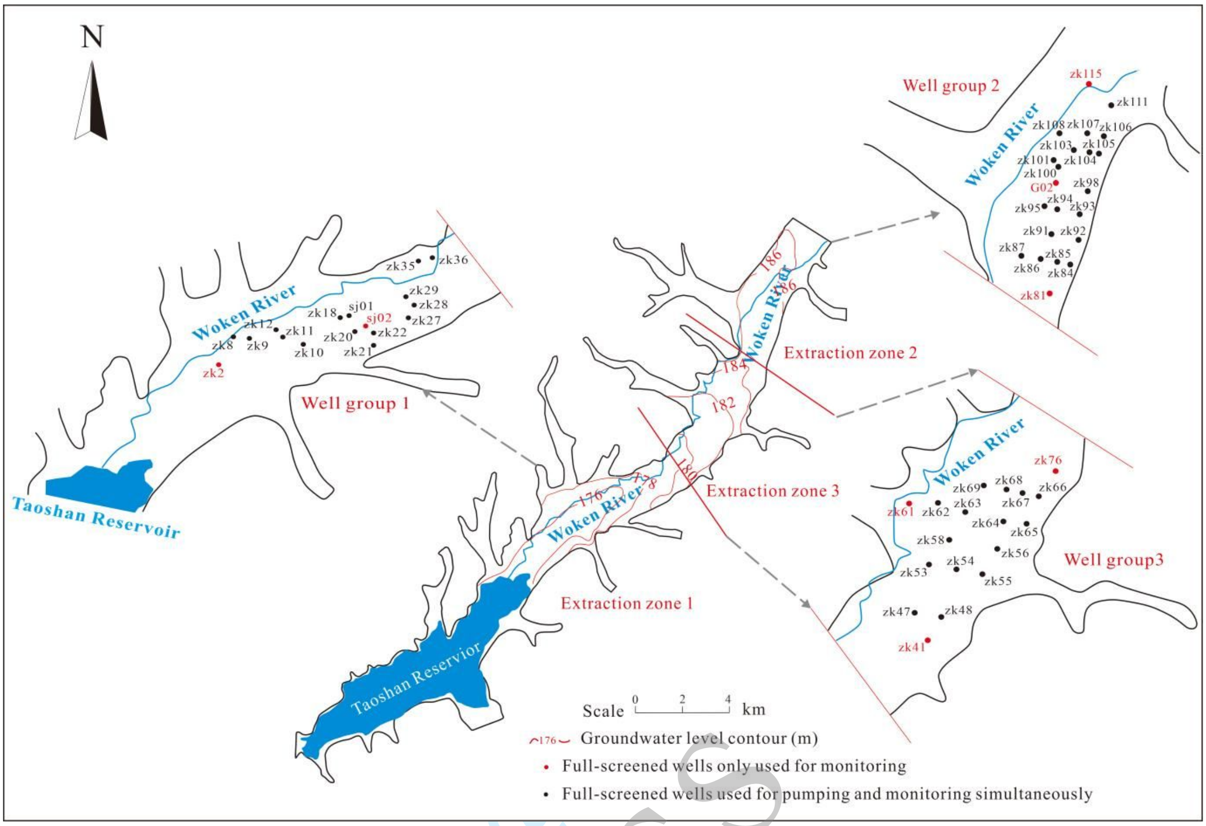

Figure 2. Groundwater flow field in the valley plain in the study area, based on the observation data for April 20, 2013 (adapted from Qi (2015)) and the locations of the pumping and observation wells associated with the three multi-well pumping tests.

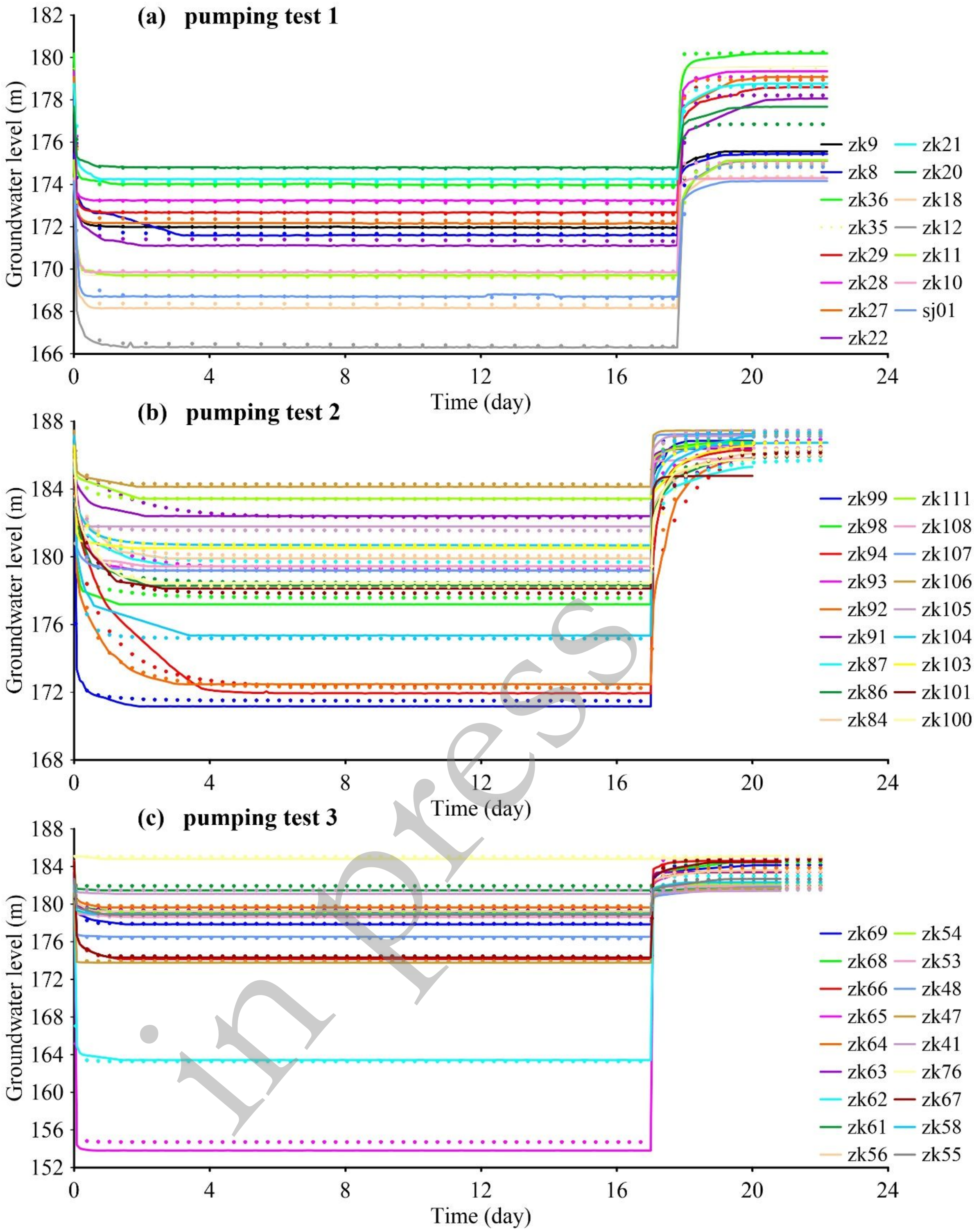

Figure 3. Observed groundwater level (solid lines) vs. model-calculated values (dotted lines) at monitoring wells during the pumping tests 1 (a), 2 (b), and 3 (c).

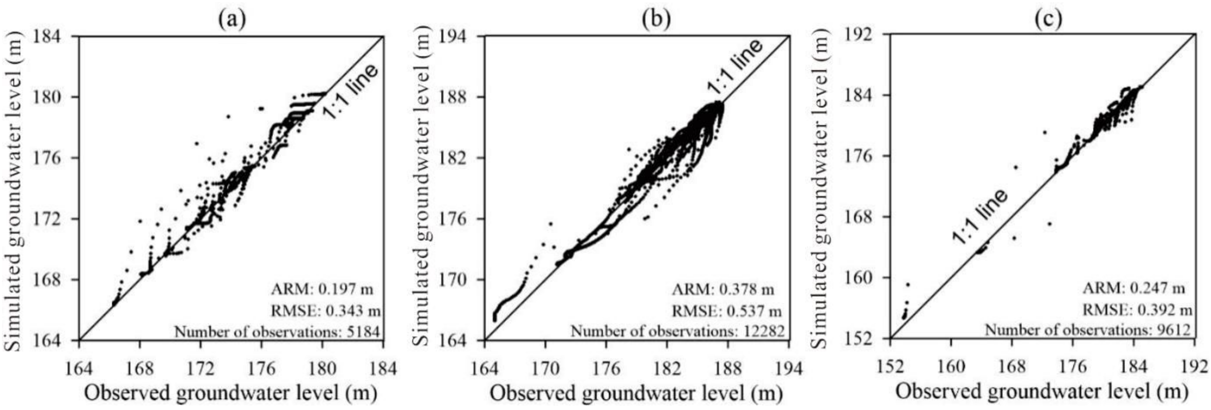

Figure 4. Comparisons of the observed and simulated hydraulic levels in the monitoring wells during pumping tests 1 (a), 2 (b), and 3 (c).

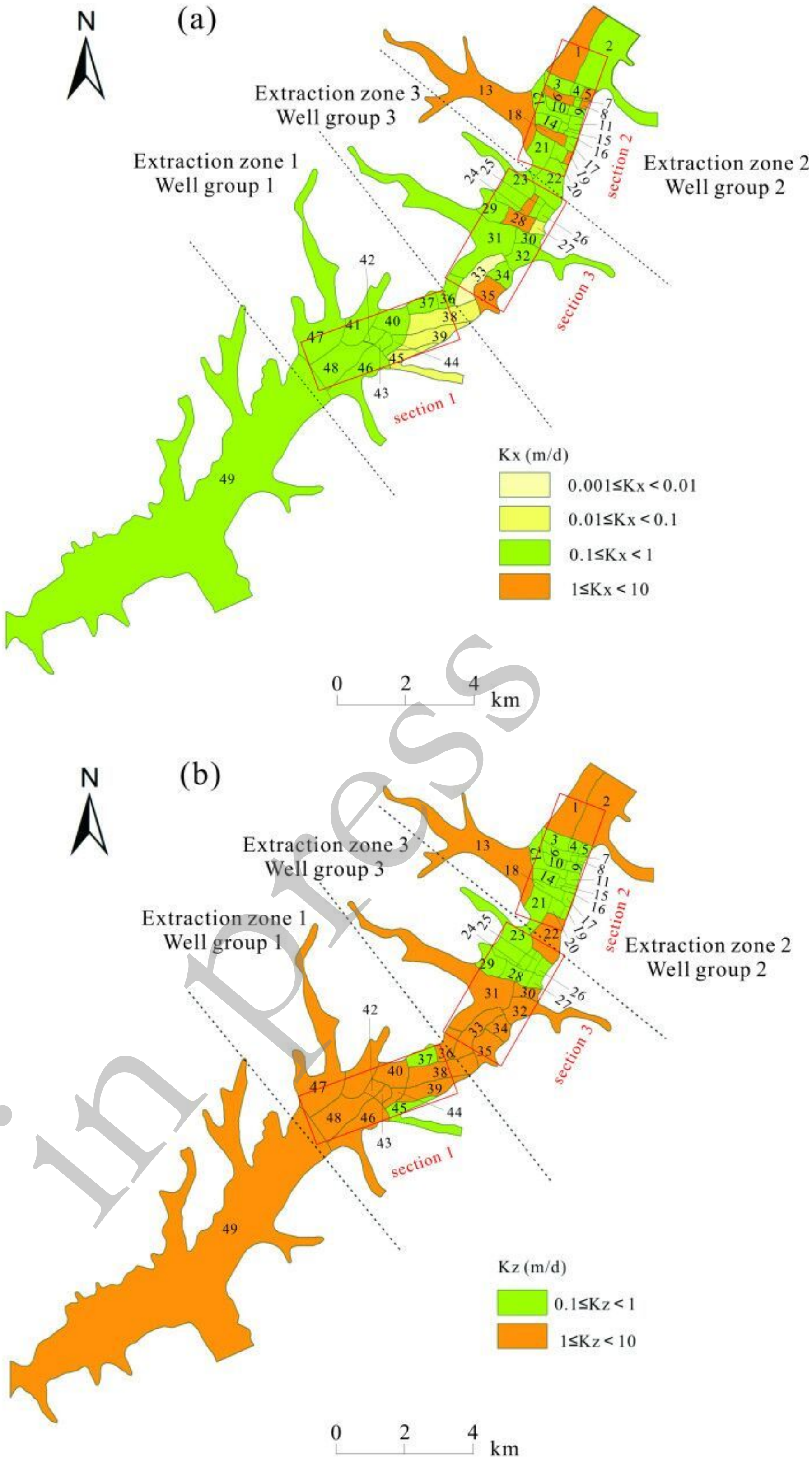

Figure 5. The maps showing the optimized horizontal hydraulic conductivity K_x (a) and vertical hydraulic conductivity K_z (b) of the first model layer, which represents the Cretaceous aquifer with well-developed fractures, in 49 zones.

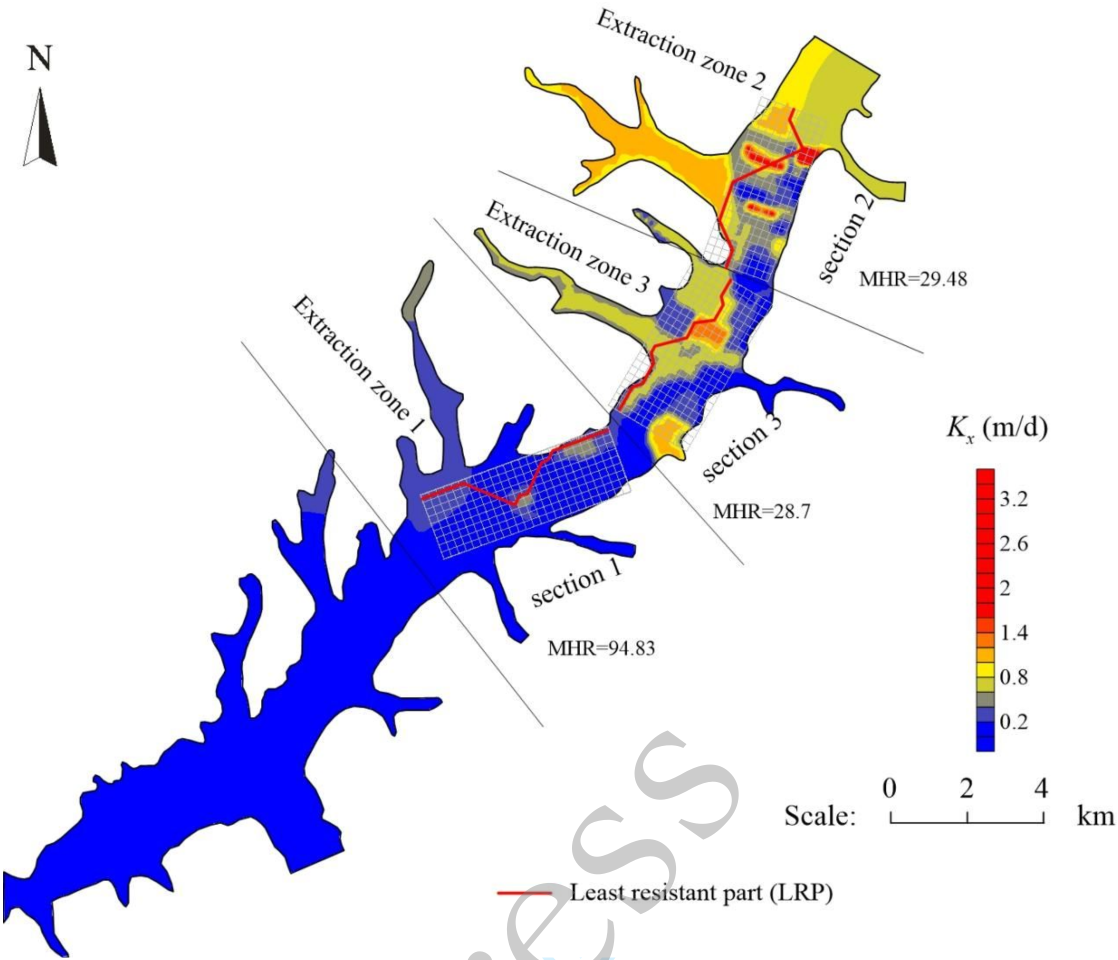

Plea**Figure 6.** The discrete grids, smoothed K_x-field, and LRPs connecting the northeastern boundary of each of the three sections to their southwestern boundary, as intercepted from the groundwater extraction regions 1, 2, and 3, respectively.